

Circumpolar variations in the chaotic nature of Southern Ocean eddy dynamics

Andrew McC. Hogg¹, Thierry Penduff², Sally E. Close^{2,4}, William K. Dewar³,
Navid C. Constantinou¹, and Josué Martínez-Moreno^{1,4}

¹Research School of Earth Sciences and ARC Centre of Excellence for Climate Extremes,

Australian National University, Canberra, Australia

²Université Grenoble Alpes, CNRS, IRD, Grenoble-INP, Institut des Géosciences de l'Environnement

(IGE), Grenoble, France

³Florida State University, Tallahassee, FL, USA

⁴Now at: Laboratoire d'Océanographie Physique et Spatiale (LOPS), University of
Brest/IFREMER/IRD/CNRS, Brest, France

Key Points:

- Monthly-to-interannual variability in the Southern Ocean eddy field is dominated by chaotic, rather than atmospherically-forced processes.
- The forced component of the eddy kinetic energy variance is significantly correlated with the local wind stress input.
- The forced changes in the eddy field lag the wind stress, with two timescales emerging: one at 4-6 months, and one at 2-3 years.

Corresponding author: Andrew McC. Hogg, Andy.Hogg@anu.edu.au

This article has been accepted for publication and undergone full peer review but has not been through the copyediting, typesetting, pagination and proofreading process, which may lead to differences between this version and the [Version of Record](#). Please cite this article as [doi: 10.1029/2022JC018440](https://doi.org/10.1029/2022JC018440).

This article is protected by copyright. All rights reserved.

19 Abstract

20 Circulation in the Southern Ocean is unique. The strong wind stress forcing and buoyancy
 21 fluxes, in concert with the lack of continental boundaries, conspire to drive the Antarctic
 22 Circumpolar Current replete with an intense eddy field. The effect of Southern Ocean eddies
 23 on the ocean circulation is significant – they modulate the momentum balance of the zonal
 24 flow, and the meridional transport of tracers and mass. The strength of the eddy field is
 25 controlled by a combination of forcing (primarily thought to be wind stress) and intrinsic,
 26 chaotic, variability associated with the turbulent flow field itself. Here, we present results
 27 from an eddy-permitting ensemble of ocean model simulations to investigate the relative
 28 contribution of forced and intrinsic processes in governing the variability of Southern Ocean
 29 eddy kinetic energy. We find that variations of the eddy field are mostly random, even
 30 on longer (interannual) timescales. Where correlations between the wind stress forcing
 31 and the eddy field exist, these interactions are dominated by two distinct timescales – a
 32 fast baroclinic instability response; and a multi-year process owing to feedback between
 33 bathymetry and the mean flow. These results suggest that understanding Southern Ocean
 34 eddy dynamics and its larger-scale impacts requires an ensemble approach to eliminate
 35 intrinsic variability, and therefore may not yield robust conclusions from observations alone.

36 Plain language summary

37 The Southern Ocean is the most turbulent part of the world's oceans. This turbulence,
 38 often referred to as *eddies*, is critical to the evolution of the Southern Ocean under climate
 39 change. But it's hard to get information about these eddies, because they occur on small
 40 scales in a large ocean basin that is poorly observed. In addition, the observational record is
 41 quite short, which makes it more difficult to use these observations to study what controls
 42 variations of these eddies. For this reason, we take an eddy-permitting ocean model, and run
 43 it 50 times with the same forcing (but a slightly different initial state). The chaotic nature
 44 of the turbulent ocean means that these model runs exhibit different evolutions. Then we
 45 use these simulations to study which eddy processes occur as a consequence of the chaotic
 46 nature of turbulence and which are forced by the external factors that are common to all
 47 model runs (such as wind stress). We conclude that monthly-to-interannual fluctuations
 48 of the Southern Ocean eddy field are dominated by chaotic processes; but that the forced
 49 variability responds to wind on particular timescales that are controlled by the mechanisms
 50 that generate ocean turbulence.

51 1 Introduction

52 The Southern Ocean is unique in the global ocean; it is the one region without continents
 53 on its zonal boundaries, giving rise to the Antarctic Circumpolar Current (ACC) that flows
 54 eastward around the globe. The ACC acts to connect the other major basins and thereby
 55 regulates climate and nutrients. The Southern Ocean region is also a place where mid-
 56 and high-latitude ventilation of the oceans occurs, leading to carbon and heat uptake and
 57 controlling deep ocean stratification (Rousselet et al., 2021; Morrison et al., 2022). However,
 58 the Southern Ocean is also poorly observed (compared with other ocean basins) and its
 59 unique properties mean that improved understanding of the dynamics of this region will
 60 important implications (with the aim of predicting future responses to climate change).

61 Another unique feature of the Southern Ocean is that it has a strong eddy field (Fu et al.,
 62 2010). This eddy field has been suggested to be important in the Southern Ocean's response
 63 to change. For example, the eddy saturation hypothesis (Hallberg & Gnanadesikan, 2006;
 64 Meredith & Hogg, 2006; Munday et al., 2013; Constantinou & Hogg, 2019) suggests that the
 65 role of eddies in facilitating vertical momentum transport acts to limit the response of ACC
 66 transport to changing winds. A similar dynamic, known as eddy compensation, describes
 67 the role of eddies in moderating the effect of wind-driven change on the Southern Ocean
 68 overturning circulation (Morrison & Hogg, 2013). Therefore, the response of mesoscale

transient motion in the Southern Ocean is likely important to characterising the dynamics of this region.

The strength of the Southern Ocean eddy field is usually characterised by extracting the kinetic energy of transient motions; referred to by oceanographers as eddy kinetic energy (EKE). It is important to highlight that EKE includes all transient motion, not just coherent vortices (Martínez-Moreno et al., 2019), and thus care needs to be taken in interpreting this metric. Eddy kinetic energy has a complex relationship with the forces that drive the ocean circulation. Meredith & Hogg (2006) found significant variations in the area-averaged eddy field in some regions, and argued for a 2-3 year lag between wind stress forcing variations and EKE anomalies that follow. Patara et al. (2016), using a realistic high-resolution ocean model found that EKE does have a lagged response to wind stress anomalies, but that this relationship varies in strength around the Southern Ocean. Idealised model studies over a wide range of parameter space (Sinha & Abernathey, 2016) have highlighted that the timescale of the perturbation is critical in determining the EKE response, with shorter perturbations having a faster, Ekman-related response. Thus, current knowledge suggests that there is a relationship between wind forcing and Southern Ocean EKE, but that the nature of this relationship needs to be clarified.

On longer timescales, it has also been proposed that EKE has increased over recent decades (Hogg et al., 2015; Martínez-Moreno et al., 2019, 2021). The robustness of this wind-EKE relationship in the Southern Ocean was recently investigated by Zhang et al. (2021), who used crossover data from satellite observations (as in Hogg et al., 2015) to better estimate the EKE on regional scales. By fine-graining these calculations it was found that only a single region (30° -wide in longitude) expressed a significant long-term trend in EKE. This finding suggests that previous characterisations of the response may have been dominated by a small number of regional events, calling into question the robustness of previous studies.

The dynamical importance of the Southern Ocean eddy field, and uncertainty over the robustness of its variability and trends, motivate a deeper investigation into the processes that control Southern Ocean eddies. A key issue here is the extent to which the eddy field purely responds to external (atmospheric) forcing, versus the role of chaotic and intrinsic variability in determining eddy energy. The fact that high-frequency eddy variability is random and chaotic is well-known, and even non-eddying ocean models can produce (a small amount of) intrinsic variability via large-scale baroclinic instability (e.g. de Verdière & Huck, 1999; Constantinou & Hogg, 2021). At longer timescales intrinsic variability can emerge from oceanic non-linearities under constant or seasonal forcing and persists under variable forcing (Leroux et al., 2018). Such intrinsic variability has a random phase (that is, it is chaotic in character); it mostly emerges at mesoscale and can cascade toward interannual time scales and $O(1000 \text{ km})$ space scales (Sérazin et al., 2018). One of the goals of this work is to characterise the spatiotemporal extent of chaotic, intrinsic, variability in determining Southern Ocean EKE.

A primary complication in understanding Southern Ocean EKE is the limitation of inference from an admittedly short satellite record; in particular, whether individual events can be attributed to forcing changes, or to intrinsic variability, or a combination of the two. In this paper, we address this question by examining the intrinsic variability of the Southern Ocean eddy field in a large ensemble of eddy-permitting ocean simulations. We use the OceaniC Chaos – ImPacts, strUcture, prediTability (OCCIPUT) ensemble of global ocean/sea-ice hindcast simulations (Penduff et al., 2014; Leroux et al., 2018), a 50-member ensemble of hindcast simulations. We examine both the intrinsic variance of the eddy field, and extract the “forced” (ensemble mean) component of the variability. This variability is examined on a circumpolar and regional basis, to better understand the regional differences and processes which contribute to the eddy field.

120 **2 Methods**

121 **2.1 The OCCIPUT ensemble**

122 The methodology employed in this study is derived from the probabilistic approach to
 123 ocean modelling outlined by Bessières et al. (2017). We use output from the OCCIPUT
 124 ensemble of 50 eddy-permitting global ocean–sea ice simulations, based on the ORCA025
 125 implementation (e.g. Barnier et al., 2006) of the NEMO modelling system (Madec, 2012).
 126 The model grid has a $1/4^\circ$ horizontal resolution and 75 geopotential levels. The approach
 127 involves:

- 128 1. The 50 ensemble members are initialized in 1960 from a single-member 21-year spinup
 129 using the Drakkar Forcing Set DFS5.2 (Dussin et al., 2016);
 130 2. The ensemble spread is seeded by activating a stochastic perturbation (Brankart et
 131 al., 2015) over one year (1960), after which the perturbation is terminated;
 132 3. The 50 ensemble members are integrated from 1960 to 2015, driven by the same real-
 133 istic atmospheric forcing function based on the ERA-40 and ERA-Interim reanalyses
 134 (Drakkar Forcing Set DFS5.2; Dussin et al. (2016)).

135 In these simulations the wind stress is computed without ocean current feedbacks, hence
 136 ensuring that the same momentum fluxes are applied to all members. We focus our analyses
 137 on the period 1980–2015, thus yielding an effective spinup duration of 41 years in each
 138 member.

139 **2.2 Estimating geostrophic eddy velocity**

140 For each ensemble member, the sea surface height, η_i , is saved as a 5-day average (where
 141 i represents the ensemble member). For each ensemble member, and at every time step,
 142 the member’s global mean sea level anomaly is subtracted at every grid point to correct for
 143 spurious terms introduced by the use of the Boussinesq approximation (Greatbatch, 1994).
 144 The model drift, which is potentially nonlinear, is then corrected for by detrending using a
 145 LOWESS filter (Cleveland, 1979) in combination with a 5th-order spline; full details of this
 146 preprocessing may be found in Close et al. (2020).

147 The sea level anomaly, η'_i , is calculated as the transient component of sea level in
 148 ensemble member i , given by

$$149 \eta'_i = \eta_i - \bar{\eta}_i, \quad (1)$$

150 where $\bar{\cdot}$ represents the temporally filtered, detrended sea level (Close et al., 2020). The sea
 151 level anomaly is then used to calculate the eddy velocity field. Surface eddy velocity in each
 152 ensemble member, $\mathbf{u}'_i = (u'_i, v'_i)$ is estimated from the detrended sea level anomaly via the
 153 geostrophic relation,

$$154 u'_i = -\frac{g}{f} \frac{\partial \eta'_i}{\partial y} \quad \text{and} \quad v'_i = \frac{g}{f} \frac{\partial \eta'_i}{\partial x}, \quad (2)$$

155 where g is the acceleration due to gravity and f is the local Coriolis parameter. Anomalous
 156 values of \mathbf{u}'_i close to coastlines are removed.

157 The surface eddy kinetic energy for each ensemble member is calculated as

$$158 E_i = \frac{1}{2}(u'^2_i + v'^2_i), \quad (3)$$

159 and subsampled at monthly temporal resolution (by taking the weighted average over each
 160 month). It is notable that E_i contains a large component of seasonal variation which dom-
 161 inates the statistics (Martínez-Moreno et al., 2022). To look at the forced response, we
 162 therefore deseasonalise E_i , by removing the climatological mean; we eliminate noise on the
 163 monthly timescale by filtering with a 4-month rolling mean. We then proceed to compute
 164 ensemble statistics from this deseasonalised EKE.

165 **2.3 Ensemble eddy statistics**

166 The eddy kinetic energy can be averaged over the N ensemble members to give the
 167 ensemble mean EKE, written as

$$168 \quad \langle E \rangle = \frac{1}{N} \sum_{i=1}^N E_i. \quad (4)$$

169 The argument can be made that, since each ensemble member is forced with identical at-
 170 mospheric conditions, the forced EKE response is captured by this ensemble mean quantity.
 171 On the other hand, the intrinsic variability of EKE in each ensemble member is found by
 172 taking the difference from the ensemble mean for each member,

$$173 \quad E_i^* = E_i - \langle E \rangle, \quad (5)$$

174 where \cdot^* is used to indicate departure from the ensemble mean. With these expressions in
 175 hand, we follow Leroux et al. (2018) to define the time-variance of the ensemble-mean EKE,

$$176 \quad \sigma_{\langle E \rangle}^2 = \frac{1}{T} \sum_{t=1}^T \left(\langle E \rangle - \overline{\langle E \rangle} \right)^2, \quad (6)$$

177 which represents the variance of the forced eddy response. For each time step, the intrinsic
 178 variance emerges from the variance of the EKE difference between ensemble mean and each
 179 member of the 50 simulations,

$$180 \quad \epsilon^2(t) = \frac{1}{N} \sum_{i=1}^N E_i^*(t)^2. \quad (7)$$

181 The fraction of intrinsic variance is then computed as the ratio of the intrinsic variance to
 182 the total variance,

$$183 \quad R_i = \frac{\overline{\epsilon^2}}{\overline{\epsilon^2} + \sigma_{\langle E \rangle}^2}. \quad (8)$$

184 When R_i approaches unity, the system is dominated by intrinsic variability, while at the
 185 limit of $R_i \rightarrow 0$ the system is solely responding to forced variability induced by atmospheric
 186 forcing.

187 To examine the relationship between the EKE (of either the ensemble mean, or from
 188 individual ensemble members) and its forcing, we are guided by previous work which em-
 189 phasises the role of wind stress in governing the eddy variability at different timescales (e.g.
 190 Hogg et al., 2015; Sinha & Abernathay, 2016). Thus, we look at the correlation coefficient,
 191 r , at a range of lags between the wind stress $|\tau|$ (which is identical for all ensemble members
 192 and has been deseasonalised similarly to E_i) and EKE. For each correlation we evaluate
 193 the statistical significance of the correlation (following, e.g. Santer et al., 2000). We first
 194 calculate the effective sample size, N_e , where

$$195 \quad N_e \equiv N \frac{1 - r_1 r_2}{1 + r_1 r_2}, \quad (9)$$

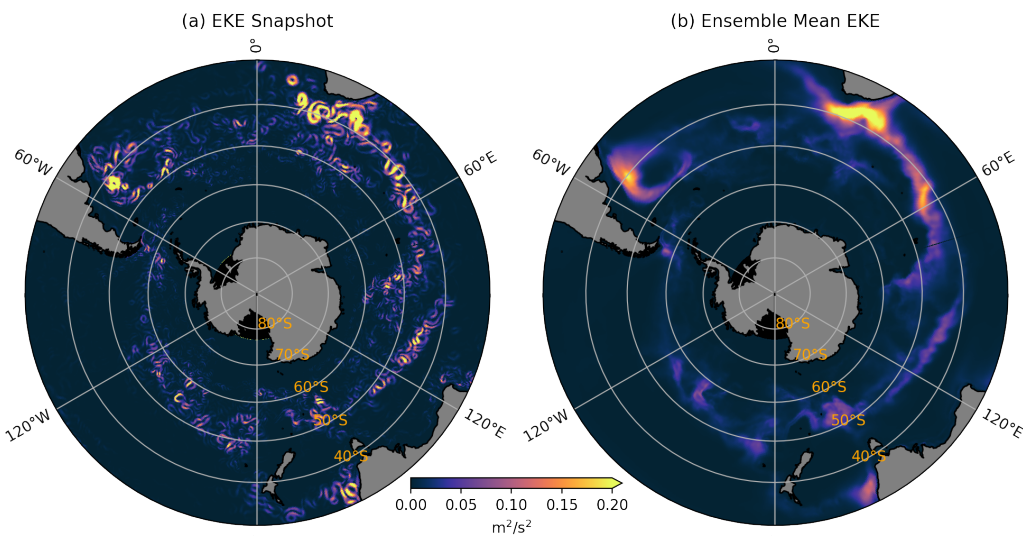
196 where N is the total number of samples (444 months for this timeseries), r_1 is the lag-1
 197 autocorrelation for EKE and r_2 is the lag-2 autocorrelation for wind stress. We use the
 198 Students t-test to infer statistical significance (at the 95%-level) based on this effective
 199 sample size, when

$$200 \quad T = \frac{r \sqrt{N_e}}{\sqrt{1 - r^2}} > 2. \quad (10)$$

201 Lagged correlation estimates indicate when this significance test is satisfied.

202 3 Results

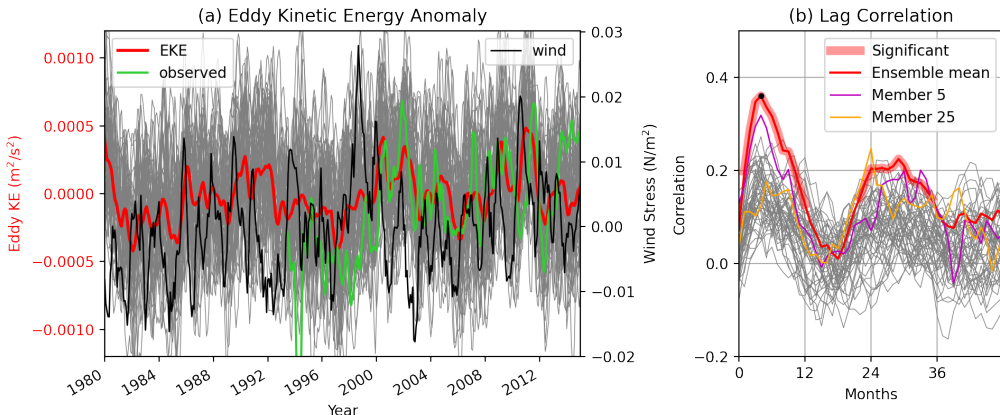
203 The intensity of the Southern Ocean eddy field is not uniform. A snapshot of eddy
 204 kinetic energy from the model used here (Fig. 1a) shows the occurrence of strong eddies
 205 which appear in the lee of subsurface topography and at the outlet from western boundary
 206 currents such as the Agulhas retroflection and Malvinas current. The same patterns are
 207 evident in the ensemble and temporal mean of the EKE ($\langle E \rangle$; Fig. 1b), although the signal
 208 of individual eddies is no longer apparent. The strongest band of EKE approximately
 209 follows the path of the Antarctic Circumpolar Current, and EKE is weak south of 60°S.
 210 The patterns of EKE in this model broadly match the regional variations of EKE observed
 211 from satellite altimetry, albeit at slightly lower intensity, as expected in an eddy-permitting
 212 model (e.g. Kiss et al., 2020).



213 **Figure 1.** (a) Snapshot (5-day average) from a single ensemble member showing Southern Ocean
 214 EKE, E_i , and (b) time-averaged ensemble mean EKE, $\langle E \rangle$.

215 For each of the 50 members of the OCCIPUT ensemble we take the EKE averaged over
 216 the entire Southern Ocean (40°–60°S), and plot the deseasonalised EKE anomalies from
 217 each ensemble member as thin grey lines in Fig. 2(a). This plot highlights the considerable
 218 spread in EKE, even when averaged over the full circumpolar belt; in other words, there
 219 is a significant component of chaotic (intrinsic) variability in the Southern Ocean eddy
 220 field. The observed EKE anomaly (calculated using data from Martínez-Moreno et al.,
 221 2022, and filtered using the same methods as model output) indicates that observations
 222 are indistinguishable from the individual ensemble members (with the exception of a short
 223 period of anomalously low EKE in the early part of the satellite record). Nonetheless, when
 224 averaged over all ensemble members (red line in Fig. 2a) the existence of a coherent (forced)
 225 component of eddy variability is revealed. Averaged over this broad region the fraction,
 226 R_i , of intrinsic variance is 0.82, confirming the visual impression that intrinsic processes
 227 dominate the variability in the eddy field averaged over the basin.

228 Although Southern Ocean EKE variability is strongly intrinsic, there remains a compo-
 229 nent of forced variability (red line in Fig. 2a). Previous studies have inferred that there is a
 230 strong contribution of wind stress forcing upon EKE, and we therefore compare the forced
 231 variability with the variations in wind stress averaged over the same circumpolar belt (black
 232 line in Fig. 2a). This comparison suggests a relationship in which wind stress leads varia-
 233 tions in EKE, consistent with previously published results (Meredith & Hogg, 2006; Hogg
 234

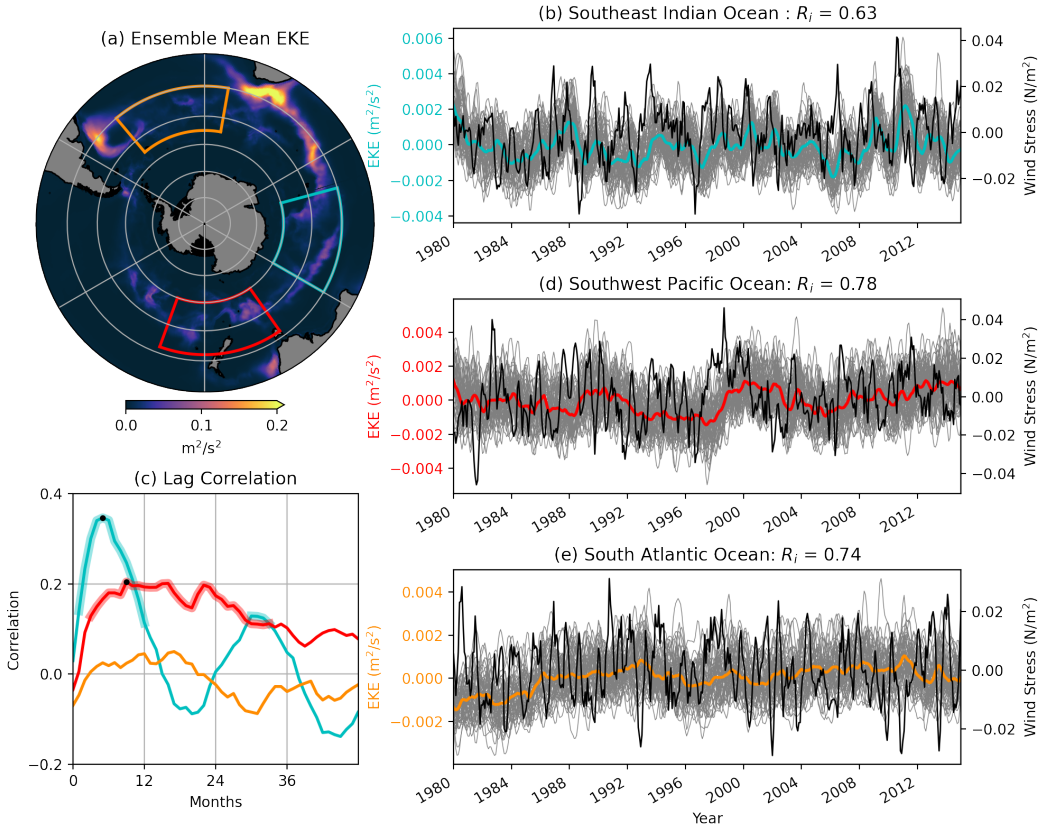


228 **Figure 2.** Eddy kinetic energy statistics over the Southern Ocean (40°S – 60°S). (a) Spatially
 229 averaged deseasonalised EKE anomaly (relative to climatology) for individual ensemble members
 230 (grey) and the ensemble mean EKE anomaly (red) and observed EKE anomaly from the satellite
 231 era (green line; calculated from Martínez-Moreno et al., 2022), along with wind stress anomaly
 232 (black); and (b) Time-lagged correlation between wind stress and EKE for the ensemble mean (red)
 233 and individual ensemble members (grey) – with two individual ensemble members highlighted in
 234 magenta and orange.

241 et al., 2015). However, the time-lagged correlations between wind stress and EKE implies
 242 that this relationship is complex. The intrinsically variable nature of Southern Ocean eddies
 243 means that for some ensemble members, there is no meaningful correlation between wind
 244 stress and eddies (grey lines in Fig 2b). On the other hand, ensemble member 5 (magenta
 245 line) has a clear (and significant; $T = 5.5$) correlation with a 4-month lag, while member
 246 25 (orange line) is weakly correlated at 6 months, and significantly correlated ($T = 4.2$) at
 247 a 24-month lag. These isolated examples highlight the differing behaviour of each ensem-
 248 ble member. The ensemble mean (red line in Fig 2b) includes a significant correlation at
 249 \sim 4 months ($T = 5.9$) and a second significant peak at \sim 30 months ($T = 3.5$). Thus, two
 250 distinct timescales of response of the Southern Ocean eddy field to wind stress are present
 251 in this model, overprinted by a dominant and complex influence of chaotic variability.

252 The ensemble of simulations shown here allow us to look in more detail at smaller
 253 regions of the Southern Ocean. Calculating the variability of EKE in a smaller region
 254 has the advantage of isolating the individual processes which may occur in differing regions
 255 (for example, stronger topographic steering in places with steep bathymetry). However, this
 256 advantage is partly offset by higher intrinsic variability; if the region of interest is sufficiently
 257 small, then an individual eddy or event can have a large influence over the EKE timeseries.
 258 In balancing these competing issues, we examine the variability within regions that span
 259 $15\text{--}20^{\circ}$ in latitude and $30\text{--}40^{\circ}$ in longitude, as shown in Figure 3(a). We analyse the EKE
 260 timeseries averaged over these boxes – including individual member EKE, ensemble mean
 261 EKE and lagged correlations between local wind stress forcing and the ensemble mean EKE
 262 in Fig. 3(b-e).

263 We first examine a region in the lee of Kerguelen Plateau in the Southeast Indian Ocean
 264 (cyan box in Fig. 3a). This region is characterised by high-frequency (\sim 1 year) variations in
 265 EKE, with a relatively large forced component (the intrinsic variance fraction, $R_i = 0.63$, is
 266 smaller than the Southern Ocean average; Fig. 3b). The forced variation is clearly evident
 267 in the timeseries of individual ensemble members; and this forced component is related
 268 to wind stress. The lag between wind stress variations and ensemble mean EKE is short



252 **Figure 3.** Eddy kinetic energy statistics within sub-regions of the Southern Ocean. (a) Map
 253 showing ensemble mean EKE, along with 3 boxes over which a regional EKE analysis is applied;
 254 (b) Regional analysis of the Southeast Indian Ocean showing ensemble mean EKE anomaly in
 255 cyan, individual ensemble members EKE anomaly in grey and local wind stress anomaly averaged
 256 over the region in black; (c) Lagged correlation of ensemble mean EKE anomaly with wind stress
 257 anomaly in each of the three regions; (d) Regional analysis of the Southwest Pacific Ocean showing
 258 ensemble mean EKE anomaly in red, individual ensemble members EKE anomaly in grey and
 259 local wind stress anomaly averaged over the region in black; and (e) Regional analysis of the South
 260 Atlantic Ocean showing ensemble mean EKE anomaly in orange, individual ensemble members EKE
 261 anomaly in grey and local wind stress averaged anomaly over the region in black. The fraction of
 262 intrinsic variance in each region is shown in the caption of panels (b), (d) and (e).

280 (~ 5 months; cyan line in Fig. 3c) with a single clear and significant peak in the lagged
 281 correlation. There is a second, weaker but significant, correlation at 30 months lag. This
 282 region highlights a regime in which the eddy field primarily responds rapidly to variations
 283 in the local wind stress.

284 In the Southwest Pacific Ocean (red box in Fig. 3a) the situation clearly differs. Here,
 285 the intrinsic variance fraction is larger than in the Southeast Indian Ocean ($R_i = 0.78$) and
 286 the timescale of the variability is much longer (Fig. 3d). The maximum values in the lag
 287 correlation occur over a broad band from 9-24 months in this region, without a single clear
 288 peak. Thus, this region varies slowly and consistently to interannual variations in wind
 289 stress, albeit with a strong chaotic component.

In the South Atlantic Ocean (orange box in Fig. 3a) the system is again dominated by intrinsic variance ($R_i = 0.74$) and is poorly correlated with wind stress forcing (Fig. 3c,e), reinforcing the circumpolar heterogeneity of the EKE response to wind. Other regions (see Fig. 4) highlight different aspects of the local eddy response; with almost no correlation with wind forcing over the Central South Pacific (Fig. 4b) or the Southwest Indian Ocean (the Agulhas meander region; Fig. 4e). In both of these regions, intrinsic variability largely dominates the signal and correlations are weak and insignificant. On the other hand, the Southeast Pacific (north of the main pathway of the ACC) shows a strong and coherent multi-year response to wind stress, with smaller intrinsic variance fraction and a peak lag at 30 months. It is notable that this region, which is north of the mean ACC pathway, has a weak EKE signal (one tenth the magnitude of the core of the ACC). The circumpolar contrasts in both EKE response times and intrinsic variability suggests that the two-timescale response seen in Fig. 2 may be created by different processes, which each dominate in different regions of the Southern Ocean.

The heterogeneity in correlations between local wind and the ensemble mean EKE ($\langle E \rangle$) shows that, where forced variability in Southern Ocean EKE occurs, it can be partly explained by variations in wind stress. However, these correlations are based purely on local wind stress – averaged over the same area as the EKE statistics. The existence of multi-year lags between the wind and the EKE suggests that local winds may not be the only source of energy for eddy generation; in particular, it is possible that energy could be advected a considerable distance downstream during this lag period. To investigate this question we now take each of the regions outlined in Fig. 3 and look at the spatial distribution of temporal correlations between wind stress and the local ensemble mean EKE (Fig. 5). To make this calculation, wind stress is first coarsened to a $4^\circ \times 4^\circ$ grid, and wind stress in each of those coarsened grid cells correlated with ensemble mean EKE at different lags. In the Southeast Indian Ocean, Fig. 3(c) shows correlation maxima at 5 months and 30 months; the spatial variation of this correlation is shown in Fig. 5(a,b) respectively. These figures highlight a key feature of Southern Ocean wind stress, which is that there are strong autocorrelations between wind stress along a line of latitude; nonetheless, the maximum correlation between wind stress and $\langle E \rangle$ occurs within the EKE-averaging region. This correlation is lower in magnitude at 30 months (consistent with Fig. 3c), but at both 5 and 30 month lags the correlation with wind upstream of the EKE-averaging region is not stronger than within the EKE-averaging region. A similar result is found in the Southwest Pacific Ocean (Fig. 5c); wind stress correlations are relatively uniform across the Pacific Ocean owing to the autocorrelation of winds, but the correlations are less circumpolar than the Southeast Indian Ocean. Importantly, there is no suggestion of a strong correlation with wind stress upstream of the EKE-averaging region. In the South Atlantic, $\langle E \rangle$ is not strongly correlated with wind stress, either in the local region or elsewhere in the Southern Ocean (Fig. 5d). Thus, these spatial maps demonstrate that, where strong forced variability in the ensemble mean EKE exists, it is most strongly linked to local wind stress, with no suggestion of upstream or remote wind input playing a strong role.

4 Discussion and Conclusions

The simulations shown here advocate for a probabilistic approach to understanding the Southern Ocean eddy field. The 50-member ensemble of eddy-permitting ocean-sea ice model simulations investigated here demonstrate that inference about the EKE response of a single ensemble member to variable forcing in a localised region is not robust, broadly consistent with the findings of Zhang et al. (2021). This point is clarified in Fig. 6 which shows a map of the intrinsic fraction of interannual variance, R_i , from eddy statistics interpolated onto a coarse ($4^\circ \times 4^\circ$) grid, with eddy contributions filtered using a 12-month rolling mean. Here, even at interannual timescales, the chaotic variance dominates over most of the band of elevated EKE in the Southern Ocean. Subpanels (b) and (c) confirm the predominance of intrinsic eddy variability at this scale, highlighting that at small ($\sim 4^\circ$) scales we can

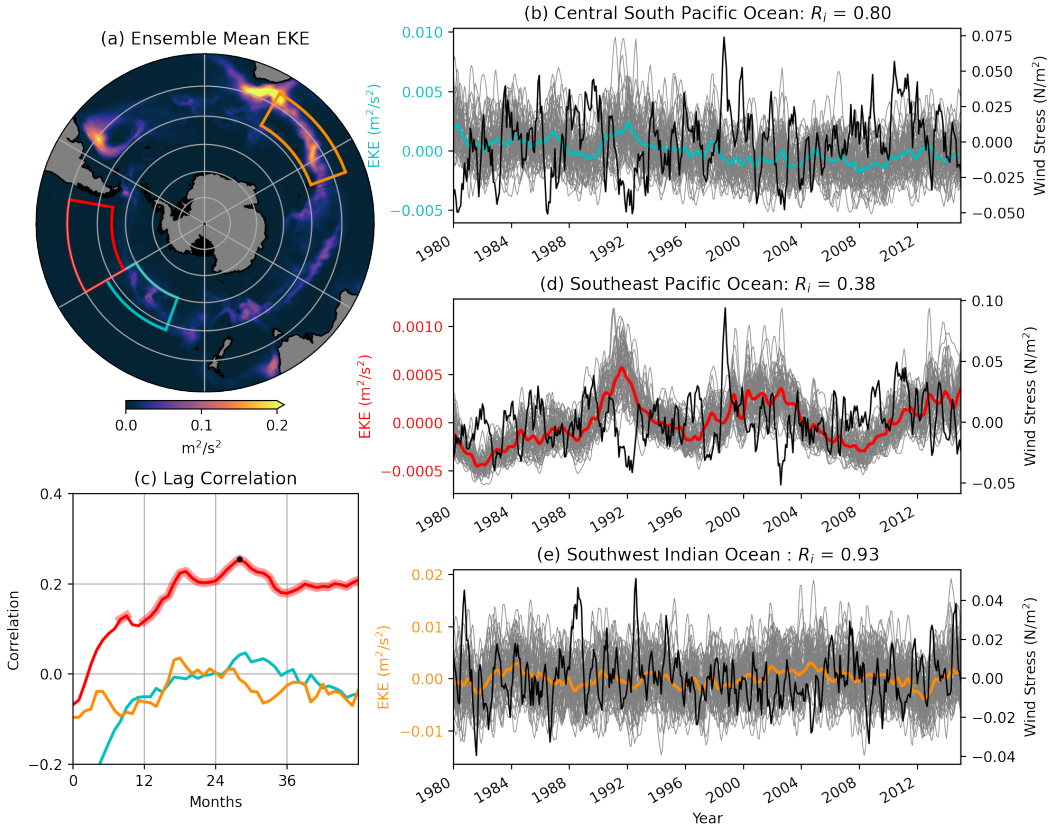
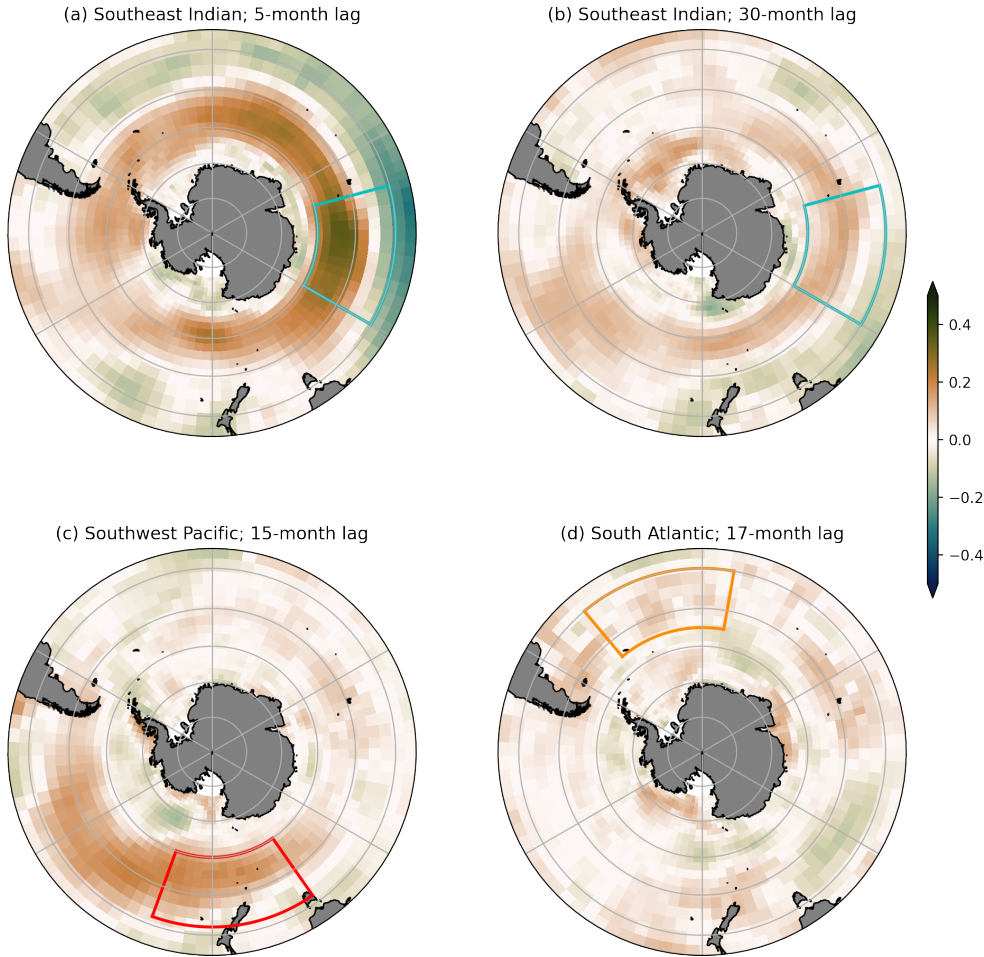


Figure 4. Eddy kinetic energy statistics within sub-regions of the Southern Ocean. (a) Map showing ensemble mean EKE, along with 3 boxes over which a regional EKE analysis is applied; (b) Regional analysis of the Central South Pacific Ocean showing ensemble mean EKE anomaly in cyan, individual ensemble members EKE anomaly in grey and local wind stress anomaly averaged over the region in black; (c) Lagged correlation of ensemble mean EKE anomaly with wind stress anomaly in each of the three regions; (d) Regional analysis of the Southeast Pacific Ocean showing ensemble mean EKE anomaly in red, individual ensemble members EKE anomaly in grey and local wind stress anomaly averaged over the region in black; and (e) Regional analysis of the Southwest Indian Ocean showing ensemble mean EKE anomaly in orange, individual ensemble members EKE anomaly in grey and local wind stress anomaly averaged over the region in black. The fraction of intrinsic variance in each region is shown in the caption of panels (b), (d) and (e).

place little reliability on the results from an individual ensemble member, or from actual observations.

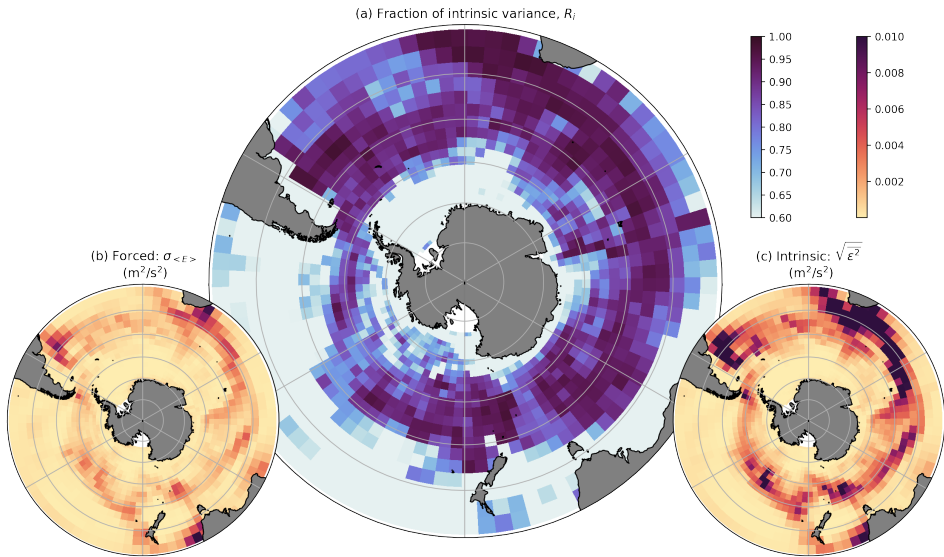
When averaged over larger regions, the fraction of intrinsic variance can be smaller than shown in Fig. 6. For example, in the Southeast Indian Ocean, in the lee of the Kerguelen Plateau, a strong and rapid response of EKE to the local wind stress can be observed (Fig. 3b,c). On the other hand, slower but significant responses in EKE are found in the Southwest Pacific Ocean, near Campbell Plateau (Fig. 3c,d). Both of these regions are locations where topography acts to sharpen and energise fronts. However, in many other regions, EKE variability appears to be almost entirely chaotic. This heterogeneity, consistent with the findings of Patara et al. (2016), acts to emphasise the differing flow regimes which are found in different parts of the Southern Ocean.



315 **Figure 5.** The spatial correlation of wind stress with $\langle E_i \rangle$ in (a) the Southeast Indian Ocean at
 316 5-month lag; (b) the Southeast Indian Ocean at 30-month lag; (c) the Southwest Pacific ocean at
 317 15-month lag and (d) the South Atlantic Ocean at 17-month lag.

370 Averaged over the entire Southern Ocean two significant timescales of correlation are
 371 found between wind stress and the ensemble mean EKE: one at 4-6 months, and the other
 372 at ~ 30 months. The rapid timescale is the expected Ekman response, in which wind stress
 373 tilts isopycnals to store available potential energy, which is then released to EKE through
 374 baroclinic instability (e.g. Sinha & Abernathey, 2016). This mechanism is the direct eddy
 375 response to wind stress changes via baroclinic instability.

376 The slower timescale is similar to that proposed by Meredith & Hogg (2006), based
 377 on a single large Southern Ocean wind event in 1999. This timescale is consistent with the
 378 topographic feedback mechanism of Hogg & Blundell (2006). Under this mechanism, the
 379 system first responds directly, via baroclinic instability, as described above. The stronger
 380 eddy field acts to increase the vertical momentum transfer which enables topography to steer
 381 the current and thereby increase the meridional component of the mean flow. Currents
 382 with a non-zonal component are more susceptible to baroclinic instability (e.g. Arbic &
 383 Flierl, 2004) which thus produces a delayed amplification of the EKE response. This second



358 **Figure 6.** (a) The interannual intrinsic variance fraction, R_i , averaged onto a $4^\circ \times 4^\circ$ grid and
 359 with a 12-month rolling mean; (b) amplitude of interannual variability due to forced processes and
 360 (c) amplitude of interannual EKE variability due to intrinsic processes.

384 mechanism describes a positive feedback between the eddy field and the mean currents which
 385 acts to enhance EKE over longer timescales.

386 The ensemble approach thus leads to the conclusion that changes in eddy activity in the
 387 Southern Ocean have a strong random character, even when averaged over a large spatial
 388 area and up to interannual time scales. This result argues for caution in interpreting obser-
 389 vations of Southern Ocean eddies, which are necessarily based on a single, short realisation
 390 of the natural world. Given that eddies are critical for the Southern Ocean circulation, this
 391 result implies that predictability of the future Southern Ocean may be weaker than previ-
 392 ously thought. The results outlined here also highlight the difficulty faced in distinguishing
 393 the processes that govern eddy dynamics in this system, and point to more systematic eddy
 394 identification and modelling studies to better isolate these processes.

395 Acknowledgments

396 AMH is grateful to the MEOM team at IGE, Université Grenoble Alpes, who supported
 397 his sabbatical and which led to this work. The results of this research have been achieved
 398 using the PRACE Research Infrastructure resource CURIE based in France at TGCC.
 399 This work is a contribution to the OCCIPUT and PIRATE projects. OCCIPUT has been
 400 funded by ANR through contract ANR-13-BS06-0007-01. PIRATE has been funded by
 401 CNES through the Ocean Surface Topography Science Team (OST-ST). WKD was funded
 402 by ANR-18-MPGA-0002 and NSF grants OCE-182956 and OCE-2023585. NCC was funded
 403 by the Australian Research Council DECRA Fellowship DE210100749. This research was
 404 undertaken with the assistance of resources and services from the National Computational
 405 Infrastructure (NCI), which is supported by the Australian Government.

406 The model output used in this study can be downloaded from the Zenodo repository
 407 at doi: 10.5281/zenodo.5835168. The full OCCIPUT model dataset is available on request
 408 (mailto:Thierry.Penduff@cnrs.fr Thierry.Penduff@cnrs.fr).

409 **References**

- 410 Arbic, B. K., & Flierl, G. R. (2004). Effects of mean flow direction on energy, isotropy, and
 411 coherence of baroclinically unstable beta-plane geostrophic turbulence. *J. Phys. Ocean.*,
 412 *34*, 77–93.
- 413 Barnier, B., Madec, G., Penduff, T., Molines, J.-M., Treguier, A.-M., Le Sommer, J., ...
 414 others (2006). Impact of partial steps and momentum advection schemes in a global
 415 ocean circulation model at eddy-permitting resolution. *Ocean Dyn.*, *56*(5), 543–567. doi:
 416 10.1007/s10236-006-0082-1
- 417 Bessières, L., Leroux, S., Brankart, J.-M., Molines, J.-M., Moine, M.-P., Bouttier, P.-A., ...
 418 Sérazin, G. (2017). Development of a probabilistic ocean modelling system based
 419 on NEMO 3.5: application at eddying resolution. *Geosci. Model Dev.*, *10*(3), 1091–1106.
 420 doi: 10.5194/gmd-10-1091-2017
- 421 Brankart, J.-M., Candille, G., Garnier, F., Calone, C., Melet, A., Bouttier, P.-A., ... Verron,
 422 J. (2015). A generic approach to explicit simulation of uncertainty in the nemo ocean
 423 model. *Geosci. Model Dev.*, *8*(5), 1285–1297. doi: 10.5194/gmd-8-1285-2015
- 424 Cleveland, W. S. (1979). Robust Locally Weighted Regression and Smoothing Scatterplots.
 425 *J. Am. Stat. Assoc.*, *74*(368), 829–836. doi: 10.1080/01621459.1979.10481038
- 426 Close, S., Penduff, T., Speich, S., & Molines, J.-M. (2020, may). A means of estimating
 427 the intrinsic and atmospherically-forced contributions to sea surface height variability
 428 applied to altimetric observations. *Progress in Oceanography*, *184*, 102314. doi: 10.1016/
 429 j.pocean.2020.102314
- 430 Constantinou, N. C., & Hogg, A. M. (2019). Eddy saturation of the Southern Ocean: a
 431 baroclinic versus barotropic perspective. *Geophys. Res. Lett.*, *46*(21), 12202–12212. doi:
 432 10.1029/2019GL084117
- 433 Constantinou, N. C., & Hogg, A. M. (2021). Intrinsic oceanic decadal variability of upper-
 434 ocean heat content. *J. Clim.*, *34*(15), 6175–6189. doi: 10.1175/JCLI-D-20-0962.1
- 435 de Verdière, A. C., & Huck, T. (1999). Baroclinic instability: An oceanic wavemaker for
 436 interdecadal variability. *J. Phys. Oceanogr.*, *29*, 893–910.
- 437 Dussin, R., Barnier, B., Brodeau, L., & Molines, J. M. (2016). The making of
 438 DRAKKAR forcing set DFS5. *DRAKKAR/MyOcean Rep. 01-04-16*. (available at
 439 https://www.drakkar-ocean.eu/publications/reports/report_DFS5v3_April2016.pdf)
- 440 Fu, L.-L., Chelton, D. B., Le Traon, P.-Y., & Morrow, R. (2010). Eddy dynamics from
 441 satellite altimetry. *Oceanography*, *23*(4), 14–25.
- 442 Greatbatch, R. J. (1994). A note on the representation of steric sea level in models that
 443 conserve volume rather than mass. *Journal of Geophysical Research: Oceans*, *99*(C6),
 444 12767–12771. doi: 10.1029/94JC00847
- 445 Hallberg, R., & Gnanadesikan, A. (2006). The role of eddies in determining the structure and
 446 response of the wind-driven Southern Hemisphere overturning: Results from the modeling
 447 eddies in the Southern Ocean (MESO) project. *J. Phys. Oceanogr.*, *36*, 2232–2252. doi:
 448 10.1175/JPO2980.1
- 449 Hogg, A. M., & Blundell, J. R. (2006). Interdecadal variability of the Southern Ocean. *J.*
 450 *Phys. Oceanogr.*, *36*, 1626–1645. doi: 10.1175/JPO2934.1
- 451 Hogg, A. M., Meredith, M. P., Chambers, D. P., Abrahamsen, E. P., Hughes, C. W., &
 452 Morrison, A. K. (2015). Recent trends in the Southern Ocean eddy field. *J. Geophys.*
 453 *Res.-Oceans*, *120*, 1–11. doi: 10.1002/2014JC010470
- 454 Kiss, A. E., Hogg, A. M., Hannah, N., Boeira Dias, F., Brassington, G. B., Chamberlain,
 455 M. A., ... Zhang, X. (2020). ACCESS-OM2 v1.0: A global ocean-sea ice model at three
 456 resolutions. *Geosci. Model Dev.*, *13*(2), 401–442. doi: 10.5194/gmd-13-401-2020
- 457 Leroux, S., Penduff, T., Bessières, L., Molines, J. M., Brankart, J. M., Sérazin, G., ...
 458 Terray, L. (2018). Intrinsic and atmospherically forced variability of the AMOC: Insights
 459 from a large-ensemble ocean hindcast. *J. Climate*, *31*(3), 1183–1203. doi: 10.1175/
 460 JCLI-D-17-0168.1
- 461 Madec, G. (2012). NEMO ocean general circulation model reference manual. *Intern. Rep.*,

- 462 27(1-386).
- 463 Martínez-Moreno, J., Hogg, A. M., England, M. E., Constantinou, N. C., Kiss, A. E., &
464 Morrison, A. K. (2021). Global changes in oceanic mesoscale currents over the satellite
465 altimetry record. *Nat. Clim. Chang.*, 11, 397403. doi: 10.1038/s41558-021-01006-9
- 466 Martínez-Moreno, J., Hogg, A. M., & England, M. H. (2022). A near-global climatology
467 of oceanic coherent eddies. *J. Geophys. Res.-Oceans*. (submitted) doi: 10.1002/essoar
468 .10506866.1
- 469 Martínez-Moreno, J., Hogg, A. M., Kiss, A. E., Constantinou, N. C., & Morrison, A. K.
470 (2019). Kinetic energy of eddy-like features from sea surface altimetry. *J. Adv. Model.
471 Earth Sy.*, 11(10), 3090-3105. doi: 10.1029/2019MS001769
- 472 Meredith, M. P., & Hogg, A. M. (2006). Circumpolar response of Southern Ocean eddy
473 activity to a change in the Southern Annular Mode. *Geophys. Res. Lett.*, 33(16). doi:
474 10.1029/2006GL026499
- 475 Morrison, A. K., & Hogg, A. M. (2013). On the relationship between Southern Ocean
476 overturning and ACC transport. *J. Phys. Oceanogr.*, 43, 140-148. doi: 10.1175/JPO-D
477 -12-057.1
- 478 Morrison, A. K., Waugh, D. W., Hogg, A. M., Jones, D. C., & Abernathey, R. P. (2022).
479 Ventilation of the Southern Ocean Pycnocline. *Ann. Rev. Mar. Sci.*, 14(1). doi: 10.1146/
480 annurev-marine-010419-011012
- 481 Munday, D. R., Johnson, H. L., & Marshall, D. P. (2013). Eddy saturation of equilibrated
482 circumpolar currents. *J. Phys. Oceanogr.*, 43, 507-532. doi: 10.1175/JPO-D-12-095.1
- 483 Patara, L., Böning, C. W., & Biastoch, A. (2016). Variability and trends in Southern Ocean
484 eddy activity in 1/12° ocean model simulations. *Geophys. Res. Lett.*, 43(9), 4517–4523.
485 doi: 10.1002/2016GL069026
- 486 Penduff, T., Barnier, B., Terray, L., Bessières, L., Sérazin, G., Grégorio, S., ... Brasseur,
487 P. (2014). Ensembles of eddying ocean simulations for climate. *CLIVAR Exchanges No.
488 65, Special Issue on High Resolution Ocean Climate Modelling*, 19(2), 26-29.
- 489 Rousselet, L., Cessi, P., & Forget, G. (2021). Coupling of the mid-depth and abyssal
490 components of the global overturning circulation according to a state estimate. *Sci. Adv.*,
491 7(21), eabf5478. doi: 10.1126/sciadv.abf5478
- 492 Santer, B. D., Wigley, T., Boyle, J., Gaffen, D. J., Hnilo, J., Nychka, D., ... Taylor, K.
493 (2000). Statistical significance of trends and trend differences in layer-average atmospheric
494 temperature time series. *J. Geophys. Res.-Atmospheres*, 105(D6), 7337–7356. doi: 10
495 .1029/1999JD901105
- 496 Sérazin, G., Penduff, T., Barnier, B., Molines, J.-M., Arbic, B. K., Müller, M., & Terray,
497 L. (2018). Inverse cascades of kinetic energy as a source of intrinsic variability: A global
498 OGCM study. *J. Phys. Oceanogr.*, 48(6), 1385-1408. doi: 10.1175/JPO-D-17-0136.1
- 499 Sinha, A., & Abernathey, R. P. (2016). Time scales of Southern Ocean eddy equilibration.
500 *J. Phys. Oceanogr.*, 46(9), 2785–2805. doi: 10.1175/JPO-D-16-0041.1
- 501 Zhang, Y., Chambers, D., & Liang, X. (2021). Regional trends in Southern Ocean eddy
502 kinetic energy. *J. Geophys. Res.-Oceans*. doi: 10.1029/2020jc016973